International Journal of Microwave and Wireless Technologies

cambridge.org/mrf

Signal distortions in circular dielectric waveguides at mm-wave frequencies

Andre Meyer and Martin Schneider

RF & Microwave Engineering Laboratory, University of Bremen, Bremen, Germany

Research Paper

Cite this article: Meyer A, Schneider M (2022). Signal distortions in circular dielectric waveguides at mm-wave frequencies. *International Journal of Microwave and Wireless Technologies* **14**, 8–18. https://doi.org/10.1017/S1759078721000209

Received: 30 October 2020
Revised: 3 February 2021
Accepted: 4 February 2021
First published online: 10 March 2021

Keywords:
Dielectric waveguide; dispersion; distortion; millimeter-wave (mm-wave); polymer microwave fiber

Author for correspondence:
Andre Meyer,
E-mail: sekretariat@hf.uni-bremen.de

Abstract

Despite the great progress in data transmission systems using dielectric waveguides (DWGs) in the millimeter-wave (mm-wave) frequency band (30–300 GHz), the signal distortions caused by DWGs have not yet been fully understood. However, such investigations would help to optimize DWGs as a transmission channel in order to further increase data rate and transmission distance of such systems without the need for more complex transceivers. Therefore, this paper presents a detailed study of the expected signal distortions caused by frequency-dependent attenuation and frequency-dependent group delay of circular DWGs at mm-wave frequencies. Based on a low-complexity digital transmission system, the effects of DWGs on the signal-to-noise ratio and the intersymbol interference at the receiver are evaluated. The figures and equations given in this paper allow the reader to easily calculate the channel properties and signal distortions for a wide range of circular DWGs without the need of finite element method solver or other time-consuming numerical simulations. Finally, design recommendations are given to minimize signal distortions for transmitting signals along DWGs.

Introduction

Since the rediscovery of dielectric waveguides (DWGs) as a medium for high data rate transmission at millimeter-wave (mm-wave) frequencies in 2010 [1], a tremendous development has been observed in this field [2, 3]. From the beginnings until today, the achievable data rate over 1 m DWG has been tripled from 12 to 36 Gb/s [4]. At the same time, the maximum transmission distance increased from 1 to 15 m [5]. In order to further increase the data rate, the required components are constantly improved. Besides the optimization of transmitter and receiver units [4, 6], the increase in data capacity of DWG systems has been mainly achieved by improving the signal-to-noise ratio (SNR) at the receiver. The use of low-loss materials or different designs (e.g. hollow core fibers) for DWGs [7–9] as well as the enhanced coupling into DWGs [10–14] ensure a low insertion loss of the transmission channel and therefore increase the SNR at the receiver. In addition to signal distortions caused by noise, a broadband signal transmitted along a DWG is also disturbed by the frequency-dependent propagation characteristics of the DWG channel. These propagation characteristics include frequency-dependent attenuation and frequency-dependent group delay (waveguide dispersion) that can lead to intersymbol interference (ISI) in digital data transmission systems. The possibility to further improve the channel capacity by reducing frequency-dependent attenuation and frequency-dependent group delay of the DWG itself has not yet been completely investigated.

In [15], the channel capacity of DWGs is approximated exemplarily for some solid and hollow core DWGs in the D-Band frequency range (110−170 GHz) based on the frequency-dependent group delay. This rough first-order approximation indicates a $1/\sqrt{l}$ relation between maximum data rate and length l of the DWG. The authors concluded that waveguide dispersion is the limiting factor in a DWG data transmission system, and not insertion loss. A similar conclusion has been drawn in [16] where the dispersion caused by frequency-dependent group delay was identified as the main limitation of the presented data transmission. However, the authors also pointed out that frequency-dependent attenuation is not negligible. In both publications, the question remains unanswered how large the effect of frequency-dependent attenuation and group delay actually is and which DWGs lead to minimal signal distortions. Although Meyer *et al.* [17] have shown that waveguide dispersion caused by frequency-dependent group delay in circular solid and hollow core DWGs can be minimized by appropriate design, it is still unclear how such a reduction would affect a transmission system in detail. Therefore, it is unknown to what extent DWGs have to be optimized to ensure negligible signal distortions. Furthermore, signal distortions caused by the frequency-dependent attenuation of the DWG, as well as its minimization, has not yet been investigated.

For this reason, this paper presents a detailed analysis of expected signal distortions that occur when data are transmitted via circular DWGs in the mm-wave frequency range. First,

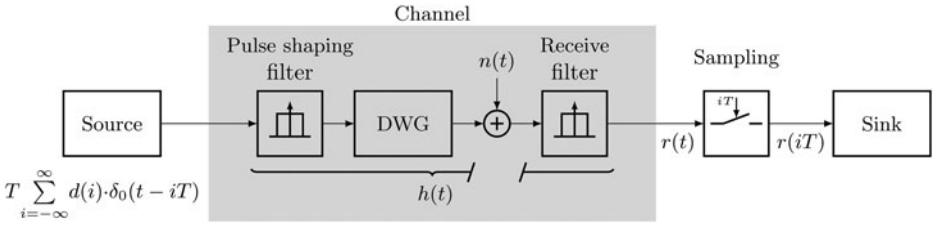

Fig. 1. Schematic representation of a low-complexity digital data transmission system using a DWG as a channel.

the data transmission system is described and the definitions of SNR and ISI for this system are introduced. Both SNR and ISI are used later to quantify the signal distortions. Subsequently, the frequency-dependent attenuation and frequency-dependent phase constant of DWGs are modeled by a Taylor series. In order to describe the frequency dependency of both values for common circular DWGs at mm-wave frequencies, a generalized analysis is given. The mathematical modeling for this analysis is specified on the basis of only two parameters, i.e. normalized frequency and normalized material properties. The general mathematical description allows the reader to directly calculate transmission properties, such as attenuation, group delay, and waveguide dispersion, of a wide range of circular DWGs that are typically used at mm-wave frequencies without the need of time consuming finite element method (FEM) simulations. Moreover, the given figures and equations can be used to calculate the expected signal distortions in a circular DWG. To determine the main cause of distortions in DWG systems, the effects of frequency-dependent attenuation and frequency-dependent group delay are analyzed separately. Finally, the combined effect of frequency-dependent attenuation and dispersion is considered, and recommendations for a DWG design are given to minimize signal distortions.

Data transmission system

To determine signal distortions along a DWG a low-complexity digital data transmission system as shown in Fig. 1 is assumed. In this communication system a data source generates an infinite pulse sequence

$$T\sum_{i=-\infty}^{\infty} d(i)\cdot\delta_0(t-iT). \tag{1}$$

where $d(i)$ represents the actual data to be transmitted. For example, $d(i)$ can be a sequence of discrete voltage values of a sampled analog signal or output values of a digital data processing system. These data points are weighted by a Dirac impulse δ_0. The time between each impulse is the sampling period T. Since the impulse sequence (1) would have an infinite bandwidth, an ideal low-pass filter

$$g(\omega)=\mathrm{rect}\left(\frac{\omega}{\omega_N}\right)=\begin{cases}1 & \text{for} \quad |\omega|<\omega_N\\ 0 & \text{else}\end{cases} \tag{2}$$

is used as pulse shaping filter to limit the signal bandwidth of the transmitted signal to $2\omega_N$. The cut-off frequency ω_N of the filter fulfills the Nyquist–Shannon sampling theorem $f_N=\omega_N/2\pi=1/2T$. After the pulse shaping filter, the band-limited signal is transmitted via DWG. Additionally, the signal is superimposed by white Gaussian distributed noise $n(t)$. To fulfill the matched filter criterion, the distorted signal is filtered at the receiver by an ideal low-pass filter (receive filter) given by (2). The filtered receive signal $r(t)$ is then sampled with the sampling period T. This results in a disturbed signal sequence at the receiver, where each received symbol $r(iT)$ can be described by

$$\begin{aligned} r(iT) &= T\sum_{k=-\infty}^{\infty} d(k)\cdot h(iT-kT)+n(iT)\\ &= \underbrace{Td(i)\cdot h(iT)}_{r_0(iT)}\\ &\quad+\underbrace{T\sum_{\substack{k=-\infty\\ k\neq 0}}^{\infty} d(k)\cdot h(iT-kT)+n(iT)}_{\Delta r(iT)} \end{aligned} \tag{3}$$

where iT represents the i-th sample point for a sampling period of $T=\pi/\omega_N$. The pulse shaping filter, the DWG as well as the receive filter are summarized as the channel impulse response $h(t)$. It can be seen that the received symbol at time iT is not only the transmitted symbol $d(i)$ disturbed by the channel impulse response (hereinafter called $r_0(iT)$), it is also superimposed by the time-shifted channel responses of all symbols $d(k)$ that were transmitted before and after the actual symbol $d(i)$ (hereinafter called $\Delta r(iT)$). This effect is well known as ISI.

In order to evaluate the signal distortions by the channel, the SNR and the ISI of the received symbols $r(iT)$ are determined. For uncorrelated random data $d(i)$ the SNR can be expressed by

$$\mathrm{SNR}=\frac{\mathrm{E}\{|r_0(iT)|^2\}}{\sigma_N^2}=\frac{\sigma_D^2}{\sigma_N^2}|h(0)|^2 \tag{4}$$

where σ_D^2 and σ_N^2 are the variances of the transmitted data sequence $d(i)$ and noise $n(iT)$. The ISI can be quantified by

$$\mathrm{ISI}=\frac{\mathrm{E}\{|r_0(iT)|^2\}}{\mathrm{E}\{|\Delta r(iT)|^2\}}=\frac{|h(0)|^2}{\sum_{\substack{k=-\infty\\ k\neq 0}}^{\infty}|h(kT)|^2} \tag{5}$$

Equations (4) and (5) depend solely on the impulse response $h(t)$ of the transmission channel including filters and DWG. Since the filter characteristics are already described by (2), a mathematical description of the DWG channel is needed to calculate the signal distortions caused by the DWG. Due to the large variety of possible diameters and materials for circular DWGs in the mm-wave frequency band, a general description of the transmission behavior of circular DWGs is presented in Section "DWG channel." Based on this description, the channel impulse response $h(t)$ is

https://doi.org/10.1017/S1759078721000209 Published online by Cambridge University Press

derived in Section "Signal distortions" and the resulting signal distortions are determined using SNR and ISI.

DWG channel

The frequency response of a DWG in the bandpass domain can be described by

$$\underline{H}_{BP}(j\omega) = e^{-\gamma(\omega)l} \tag{6}$$

where $\gamma(\omega)$ is the frequency-dependent propagation constant

$$\gamma(\omega) = \alpha(\omega) + j\beta(\omega) \qquad \alpha, \beta \in \mathbb{R}, \tag{7}$$

l the length of the waveguide and j the imaginary unit. The attenuation per unit length of an electromagnetic wave propagating along the DWG is characterized by the attenuation constant α whereas the phase change per unit length is described by the phase constant β. In practice, both constants are frequency-dependent. These frequency dependencies cause signal distortions while transmitting data along such a waveguide. To describe the frequency dependency mathematically, in this paper, real and imaginary parts of the propagation constant are approximated by a Taylor series. The Taylor series is calculated at the center frequency ω_0 of the transmitted signal:

$$\begin{aligned} &\tilde{\gamma}(\omega) = \tilde{\alpha}(\omega) + j\tilde{\beta}(\omega) \qquad \text{with} \\ &\tilde{\alpha}(\omega) = \alpha_0 + \alpha_1(\omega - \omega_0) \\ &\tilde{\beta}(\omega) = \beta_0 + \beta_1(\omega - \omega_0) + \beta_2(\omega - \omega_0)^2 \end{aligned} \tag{8}$$

and

$$\gamma_0 = \alpha_0 + j\beta_0, \quad \gamma_1 = \alpha_1 + j\beta_1, \quad \gamma_2 = j\beta_2 \tag{9}$$

For the attenuation constant α, the Taylor coefficients are

$$\alpha_0 = \alpha(\omega_0), \quad \alpha_1 = \left.\frac{d\alpha}{d\omega}\right|_{\omega=\omega_0} \tag{10}$$

The coefficient α_0 corresponds to the attenuation per unit length at the center frequency ω_0. The coefficient α_1 represents the first-order frequency dependency of the attenuation in the frequency range around the center frequency ω_0. For the phase constant β, the Taylor coefficients are

$$\beta_0 = \beta(\omega_0), \quad \beta_1 = \left.\frac{d\beta}{d\omega}\right|_{\omega=\omega_0}, \quad \beta_2 = \frac{1}{2}\left.\frac{d^2\beta}{d\omega^2}\right|_{\omega=\omega_0} \tag{11}$$

where β_0 corresponds to the phase per unit length, β_1 characterizes the group delay $\tau_g(\omega_0)$ per unit length, and β_2 is a measure for the waveguide dispersion at the center frequency. The approximation of the attenuation constant and the phase constant using a Taylor series of first and second order has been found to be highly accurate for relative bandwidths up to 5–10%. For most DWGs, a larger relative bandwidth (up to $\approx$30%) would result in a frequency dependency of $\alpha(\omega)$ and $\beta(\omega)$ that is slightly higher than the frequency dependency calculated by the Taylor approximation in this paper.

The transmission behavior of a DWG and consequently its propagation constant $\gamma(\omega)$ depends on the geometry and materials used as well as the operating frequency. In case of circular DWGs, the diameter D of the core in relation to the free-space wavelength λ_0 significantly influences the transmission behavior. To illustrate this effect, the electric field $\mathbf{E}$ of the fundamental mode HE_{11} in a circular DWG is shown for different wavelengths related to its diameter in Fig. 2. The figure shows the cross section of a circular DWG consisting of a core with a diameter D and a relative permittivity $\varepsilon_{r,1}$ surrounded by a cladding with the relative permittivity $\varepsilon_{r,2}$. At low frequencies, meaning large wavelengths in relation to the DWG diameter ($D/\lambda_0 \ll 1$), the field of the fundamental mode HE_{11} spreads widely into the cladding material. With increasing frequency, the field is further concentrated within the core of the DWG until the mode propagates almost completely in the core ($D/\lambda_0 \gg 1$). In the mm-wave frequency range, DWGs are usually operated with a diameter smaller or approximately equal to the free space wavelength ($D/\lambda_0 \approx 1$). Thus, the fundamental mode propagates in core and cladding. The ratio of the field in the core as well as in the cladding significantly influences the attenuation and phase behavior of a signal transmitted along a DWG. Since this ratio depends on the frequency, the attenuation and phase behavior can be strongly frequency-dependent, which in turn leads to signal distortions. In order to enable a general description of the propagation characteristics of various DWGs at different frequencies, Snitzer introduced the normalized frequency V and the material ratio Δ for circular DWGs [18]:

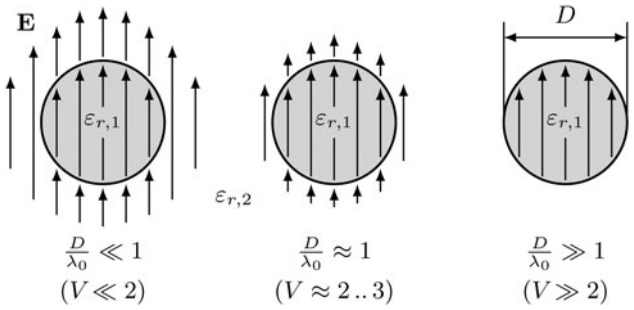

Fig. 2. Illustration of the *E*-field distribution **E** of the fundamental mode HE_{11} in a DWG at different wavelengths λ_0 related to its diameter *D*.

$$V = \frac{\omega}{c_0}\frac{D}{2}\sqrt{\varepsilon_{r,1} - \varepsilon_{r,2}} \tag{12}$$

$$\Delta = \frac{\varepsilon_{r,1} - \varepsilon_{r,2}}{\varepsilon_{r,2}} \tag{13}$$

This allows a comparison of DWGs with different diameters and materials at different frequencies, despite the large number of possible design variations. Furthermore, the normalized frequency V allows a clear classification of single-mode and multi-mode waveguides. Circular waveguides with a combination of core diameter, core and cladding material that fulfill $V < 2.405$ for a certain frequency are single-mode DWGs. Normalized frequencies of $V \geq 2.405$ indicate multi-mode DWGs. In the following, the normalized frequency V and the material ratio Δ are used to derive a general description of the Taylor coefficients α_0, α_1 and β_0, β_1, and β_2. This allows the reader to calculate these coefficients for a particular application without the need for FEM simulation tools or other complex numerical calculations.

https://doi.org/10.1017/S1759078721000209 Published online by Cambridge University Press

Attenuation constant

The attenuation constant $\alpha(\omega)$ of DWGs depends not only on the materials used for core and cladding, but also on the field distribution in both regions. For circular DWGs, the attenuation constant can be calculated by

$$\alpha(\omega) = \frac{\pi}{\lambda_0}\left(\sqrt{\varepsilon_{r,1}} R_1 \tan\delta_1 + \sqrt{\varepsilon_{r,2}} R_2 \tan\delta_2\right) \tag{14}$$

where $\tan\delta_1$, $\tan\delta_2$ are the material loss factors and R_1, R_2 are the geometric loss factors of core and cladding, respectively [19] (pp. 339), with

$$R_i = \frac{\int_{A_i} \mathbf{E}_i \cdot \mathbf{E}_i^* \, dA}{\sqrt{\frac{\mu_0}{\varepsilon_0 \varepsilon_{r,i}}}\left[\int_{A_1} \mathbf{E}_1 \times \mathbf{H}_1^* \, dA + \int_{A_2} \mathbf{E}_2 \times \mathbf{H}_2^* \, dA\right]}. \tag{15}$$

The geometric loss factors R_1 and R_2 represent the ratio between the power dissipation due to dielectric losses and the time-average power flow in core and cladding, respectively. $\mathbf{E}_1$, $\mathbf{H}_1$ and $\mathbf{E}_2$, $\mathbf{H}_2$ are the electric and magnetic vector fields of the fundamental mode HE_{11} in the core area A_1 and in the cladding area A_2, respectively. Both geometric loss factors R_1, R_2 can by normalized with respect to V and Δ. Their respective values have been analytically calculated from the numerical solution of the dispersion relation for circular DWGs as described in [19] (pp. 137). The obtained values for R_1 and R_2 are shown in Fig. 3(a) in dependency of the normalized frequency V for typical material ratios of Δ in the mm-frequency range. It can be seen that with increasing frequency the proportion of the wave in the core region increases (R_1 increases, R_2 decreases). Since the cladding material has a lower permittivity than the core material, and thus usually a lower loss factor, it seems desirable to design DWGs with the lowest possible values of R_1 and the highest possible values of R_2. However, for low values of R_1 waves are weakly guided by the DWG which leads to unwanted radiation or mode coupling in case of discontinuities like bends. For this reason, higher values of R_1 ($V \approx 2$–3) in combination with low-loss core materials are preferred in mm-wave applications.

From (10) and (14), the Taylor coefficient α_0 at a certain frequency $V_0 = V(\omega_0) = (\omega_0/c_0)(D/2)\sqrt{\varepsilon_{r,1} - \varepsilon_{r,2}}$ and therefore the attenuation of a DWG ($20\log(e^{\alpha_0 l})$ in dB) can be calculated by

$$\alpha_0 = \frac{\omega_0}{2c_0}\sqrt{\varepsilon_{r,1}}\left[R_1(V_0)\tan\delta_1 + \frac{R_2(V_0)}{\sqrt{1+\Delta}}\tan\delta_2\right] \tag{16}$$

Following the same procedure the Taylor coefficient α_1 and therefore the change of the attenuation over frequency can by calculated by

$$\alpha_1 = \frac{\sqrt{\varepsilon_{r,1}}}{2c_0}\left[\tan\delta_1\left(V_0\frac{dR_1}{dV}\bigg|_{V=V_0} + R_1(V_0)\right) + \frac{\tan\delta_2}{\sqrt{\Delta+1}}\left(V_0\frac{dR_2}{dV}\bigg|_{V=V_0} + R_2(V_0)\right)\right] \tag{17}$$

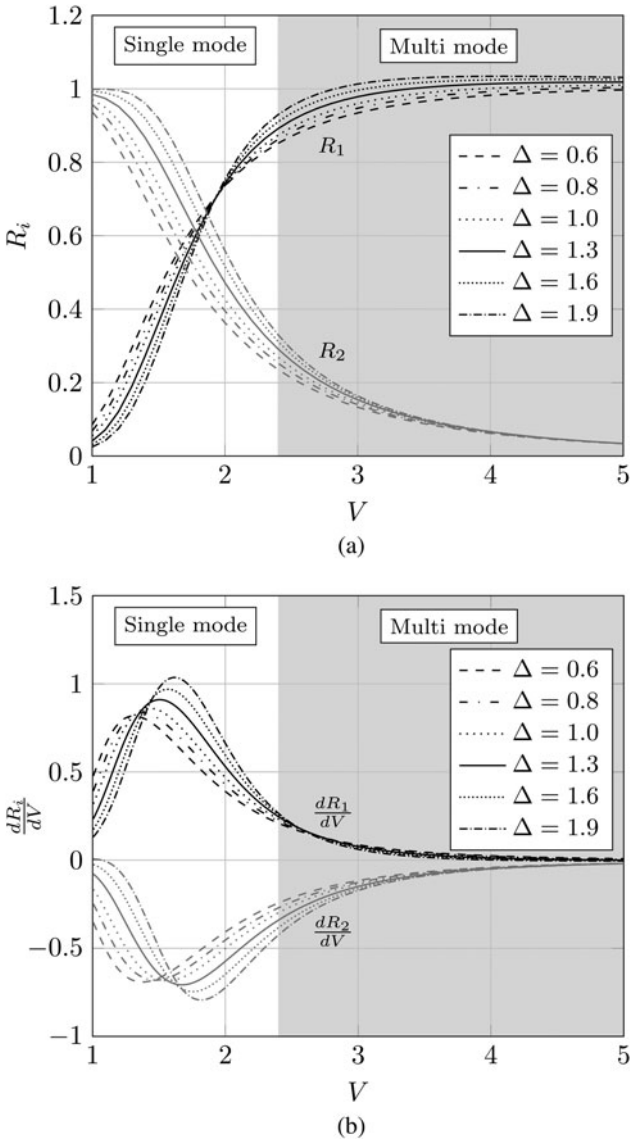

Fig. 3. Geometric loss factors R_1, R_2 (a) and their respective derivatives dR_1/dV, dR_2/dV (b) as a function of the normalized frequency V for different material ratios Δ.

It can be seen that α_1 depends not only on the geometric loss factors R_1 and R_2, but also on their derivatives dR_1/dV and dR_2/dV. The derivatives for typical material ratios Δ are shown in Fig. 3(b) as a function of the normalized frequency V. Due to the negative values of the derivative of R_2, it seems possible to compensate for the frequency-dependent attenuation by appropriate material selection. However, such a minimization of α_1 can only be achieved with a loss factor of the cladding material ($\tan\delta_2$) significantly higher than the loss factor of the core ($\tan\delta_1$) for typical material ratios Δ in the mm-wave frequency range. This would lead to a considerably higher insertion loss of the DWG. For this reason, α_1 is significantly influenced by the permittivity and loss factor of the DWG core in practice.

With the help of (16) and (17) as well as Figs 3(a) and 3(b), the Taylor coefficients α_0 and α_1 can be directly calculated for a wide range of DWGs in the mm-wave frequency range. In Table 1 these coefficients are given exemplarily for single-mode DWGs ($V_0 = 2.4$) with air cladding ($\varepsilon_{r,2} = 1$, $\tan\delta_2 = 0$) and cores made of Teflon (PTFE), polyethylene (PE), and polystyrene (PS). Comparing

https://doi.org/10.1017/S1759078721000209 Published online by Cambridge University Press

the PTFE and the PE waveguide, it can be seen that the higher core permittivity of PE not only increases the transmission losses (e.g. from 3.1 to 3.5 dB/m at 140 GHz), it also increases their frequency dependency. In combination with a high loss tangent (see PS in Table 1), the frequency dependency is highly increased. Since it is still unclear how this frequency dependency affects a signal transmitted via DWG, the coefficients α_0 and α_1 are used in Section "Signal distortions" to calculate the signal distortions caused by the frequency-dependent attenuation of circular DWGs.

Phase constant

Similar to the attenuation constant $\alpha(\omega)$ the phase constant $\beta(\omega)$ depends on the materials and field distributions in core and cladding. The phase constant is given by

$$\beta(\omega) = \frac{2\pi}{\lambda_g} = \frac{\omega}{c_0}\sqrt{\varepsilon_{r,eff}(\omega)} \tag{18}$$

where λ_g is the guided wavelength and $\varepsilon_{r,eff}$ is the effective relative permittivity with $\varepsilon_{r,2} \leq \varepsilon_{r,eff} \leq \varepsilon_{r,1}$. The effective relative permittivity is normalized by

$$B(V) = \frac{\varepsilon_{r,eff}(V) - \varepsilon_{r,2}}{\varepsilon_{r,1} - \varepsilon_{r,2}} \tag{19}$$

which is referred as the normalized phase constant that ranges between values of 0 and 1 [19] (p. 61). The normalized phase constant B can be used as a measure of the field concentration in core and cladding. It is shown as a function of the normalized frequency V for different values of Δ in Fig. 4(a). From (11), (18), and (19), the Taylor coefficient β_0 at a certain normalized frequency V_0 and therefore the phase change per unit length at the center frequency ω_0 can be calculated by

$$\beta_0 = \frac{2V_0}{D}\sqrt{B(V_0) + \frac{1}{\Delta}} \tag{20}$$

Following the same procedure the Taylor coefficient β_1, namely the group delay per unit length, can by calculated by

$$\beta_1 = \frac{\sqrt{\varepsilon_{r,1} - \varepsilon_{r,2}}}{2c_0} \cdot D\left.\frac{d\beta}{dV}\right|_{V=V_0} \quad \text{with}$$

$$\frac{d}{dV}\beta(V) = \frac{2\left(\frac{1}{\Delta} + B(V)\right) + V\frac{d}{dV}B(V)}{D\sqrt{B(V) + \frac{1}{\Delta}}} \tag{21}$$

By multiplying the derivative of β with diameter D, a normalized value for the first-order frequency dependency of the phase constant is obtained which only depends on V and Δ. This value is shown as a function of V for different values of Δ in Fig. 4(b). From (21) and Fig. 4(b) it can be seen that β_1 and therefore the group delay τ_g varies strongly over frequency. In case of a broadband signal that is transmitted along such a waveguide, the different frequency components of this signal reach the receiver at different times. This effect is known as waveguide dispersion. To reduce the waveguide dispersion, the group delay should therefore be flat over frequency. According to Fig. 4(b) this is only possible for certain normalized frequencies in a range of $2 < V < 3$ or $V \to \infty$.

The waveguide dispersion per unit length of a DWG is described by the Taylor coefficient

$$\beta_2 = \frac{1}{2}\frac{D(\varepsilon_{r,1} - \varepsilon_{r,2})}{4c_0^2} \cdot D\left.\frac{d^2\beta}{dV^2}\right|_{V=V_0} \quad \text{with}$$

$$\frac{d^2}{dV^2}\beta(V) = \frac{V\frac{d^2}{dV^2}B(V) + 2\frac{d}{dV}B(V)}{D\sqrt{B(V) + \frac{1}{\Delta}}} - \frac{V\left(\frac{d}{dV}B(V)\right)^2}{2D\left(B(V) + \frac{1}{\Delta}\right)^{3/2}} \tag{22}$$

Table 1. Taylor coefficients α_0 and α_1 as well as β_0, β_1, and β_2 for some exemplarily chosen DWGs with air cladding ($\varepsilon_{r,2} = 1$, $\tan\delta_2 = 0$)

Material		f_0 in GHz	D in mm	α_0 in 1/m	α_1 in s/m	β_0 in 1/m	β_1 in s/m	β_2 in s^2/m^2
single − mode ($V_0 = 2.4$)	PTFE ($\varepsilon_{r,1} = 2$, $\tan\delta_1 = 2 \times 10^{-4}$)	80	2.86	0.21	6.4×10^{-13}	2015	5.0×10^{-9}	2.4×10^{-22}
		140	1.64	0.36	6.4×10^{-13}	3530	5.0×10^{-9}	1.3×10^{-22}
		240	0.95	0.62	6.4×10^{-13}	6041	5.0×10^{-9}	8.3×10^{-23}
	PE ($\varepsilon_{r,1} = 2.3$, $\tan\delta_1 = 2 \times 10^{-4}$)	80	2.51	0.23	7.1×10^{-13}	2091	5.5×10^{-9}	2.6×10^{-22}
		140	1.43	0.40	7.1×10^{-13}	3656	5.5×10^{-9}	1.5×10^{-22}
		240	0.84	0.69	7.1×10^{-13}	6282	5.5×10^{-9}	7.9×10^{-23}
	PS ($\varepsilon_{r,1} = 2.5$, $\tan\delta_1 = 1 \times 10^{-3}$)	80	2.34	1.21	3.7×10^{-12}	2139	5.8×10^{-9}	2.5×10^{-22}
		140	1.34	2.12	3.7×10^{-12}	3746	5.8×10^{-9}	1.3×10^{-22}
		240	0.78	3.62	3.7×10^{-12}	6416	5.8×10^{-9}	8.2×10^{-23}
min.dispersion ($V_0 = 2.62$)	PTFE ($\varepsilon_{r,1} = 2$, $\tan\delta_1 = 2 \times 10^{-4}$)	80	3.13	0.22	6.0×10^{-13}	2060	5.0×10^{-9}	-1.6×10^{-24}
		140	1.79	0.38	6.0×10^{-13}	3605	5.0×10^{-9}	-1.7×10^{-24}
		240	1.04	0.65	6.0×10^{-13}	6174	5.0×10^{-9}	1.8×10^{-24}

https://doi.org/10.1017/S1759078721000209 Published online by Cambridge University Press

that has been derived from (11), (18), and (19). Multiplying the second derivative of β with diameter D yields a normalized value for the second order frequency dependency which only depends on V and Δ (shown in Fig. 4(c)). By using (20)–(22) as well as Fig. 4(a)–4(c), the Taylor coefficients β_0, β_1, and β_2 can now be directly calculated for a wide range of DWGs in the mm-wave frequency range. From (22) and Fig. 4(c) it can be seen that the dispersion vanishes completely ($\beta_2 = 0$) for certain DWG designs. Thus, it is possible to realize dispersion-minimized circular DWGs in the normalized frequency range $2.5 < V < 2.8$. Air-clad PTFE waveguides, for example, with core diameters of $D = 3.13$ mm, $D = 1.79$ mm, and $D = 1.04$ mm have negligible dispersion at 80 GHz, 140 GHz, and 240 GHz, respectively ($V = 2.62$, $\Delta = 1$) (see Table I). Due to the rounded diameter values, the dispersion minimum is not precisely obtained, but a comparison between the single-mode DWGs and the dispersion-optimized DWG in Table I shows that the Taylor coefficient β_2 is considerably lower. It can be observed that dispersion-minimized designs are all multi-mode waveguides ($V \geq 2.405$). In order to benefit from the low waveguide dispersion, it might be necessary to reduce the modal dispersion of these DWGs as described in [20]. However, one might also ask the question whether it is necessary to reduce the dispersion β_2 to zero to obtain negligible signal distortions. For this reason, the Taylor coefficient β_2 is used in Section "Signal distortions" to calculate the signal distortions caused by waveguide dispersion of circular DWGs.

Signal distortions

According to Heaviside [21] a channel is considered free of distortion if its propagation constant fulfills

$$\tilde{\gamma}_{opt}(\omega) = \alpha_0 + j\beta_1\omega. \tag{23}$$

Since this condition cannot be fulfilled by a DWG, the distortions to be expected when transmitting a signal via DWG are analyzed in the following. To evaluate DWGs as communication channels, the baseband ($\omega_0 = 0$) channel impulse response $h(t)$ is used. The baseband impulse response can be determined by inverse Fourier transformation $\mathcal{F}^{-1}$ of the baseband frequency transfer function

$$\underline{H}_{BB}(j\omega) = \begin{cases} e^{-(\gamma_0+\gamma_1\omega+\gamma_2\omega^2)l} & \text{for} \quad |\omega| \leq \omega_N \\ 0 & \text{else} \end{cases} \tag{24}$$

where γ_0, γ_1, and γ_2 are the complex coefficients of the approximated propagation constant $\tilde{\gamma}(\omega)$ given in (9). As described in Section "Data transmission system," a band-limited signal is assumed that is caused by an ideal low-pass filter as transmit and receive filter (see equation (2)). Thus, the baseband impulse response is

$$h(t) = \mathcal{F}^{-1}\left\{\underline{H}_{BB}(j\omega)\right\} = \frac{1}{2\pi}\int_{-\omega_N}^{\omega_N} e^{-\tilde{\gamma}(\omega)l} \cdot e^{j\omega t} d\omega \tag{25}$$

For an analytical description of the impulse response $h(t)$, the solution of (25) is separated into two parts. First, only distortions caused by a frequency-dependent attenuation are taken into account. In the second part, distortions due to a frequency-dependent phase constant, namely the dispersion, are considered.

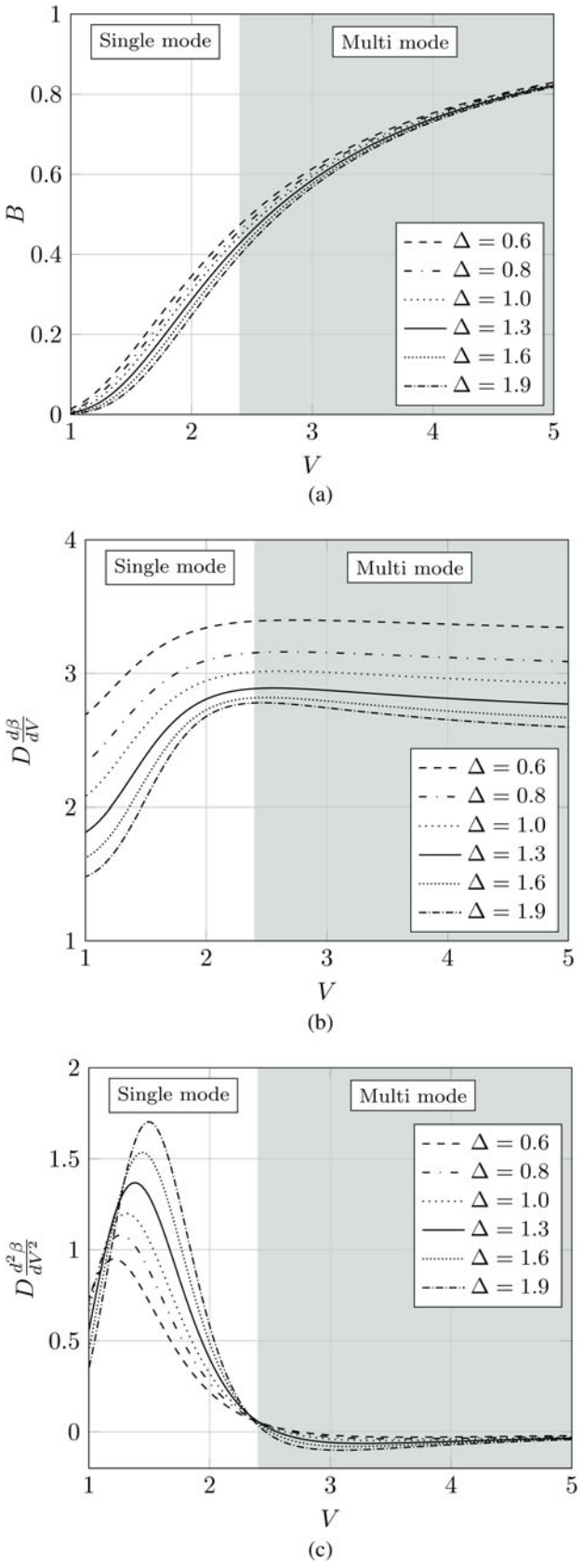

Fig. 4. Normalized phase constant B (a) as well as the first and second derivatives D ($d\beta/dV$) (b) and $D(d^2\beta/dV^2)$ (c) as a function of the normalized frequency V for different material ratios Δ.

https://doi.org/10.1017/S1759078721000209 Published online by Cambridge University Press

Distortions caused by attenuation

The frequency-dependent attenuation of DWGs is modeled by the Taylor coefficients α_0 and α_1. Therefore, the baseband frequency response of the DWG given in (24) simplifies to

$$\underline{H}_{BB}(j\omega) = \begin{cases} e^{-(\gamma_0+\gamma_1\omega)l} & \text{for} \quad |\omega| \leq \omega_N \\ 0 & \text{else} \end{cases} \tag{26}$$

By applying the inverse Fourier transform according to (25), the baseband impulse response of the DWG channel is obtained:

$$h(t) = \frac{T}{\pi}\frac{\sin\left[(j\gamma_1 l + t)\omega_N\right]}{j\gamma_1 l + t} e^{-\gamma_0 l} \tag{27}$$

This impulse response can now be used to determine the SNR and the ISI caused by the frequency-dependent attenuation of a DWG. For this considerations the Taylor coefficient β_1 is set to zero, since it only represents a time shift (namely by the group delay τ_g) of the impulse response $h(t)$ and, therefore, does not affect SNR and ISI.

Following equation (4) the SNR depends on the magnitude squared of the impulse response of the wanted signal $|h(0)|^2$. For a DWG channel with frequency-dependent attenuation follows:

$$|h(0)|^2 = \frac{1}{\omega_N^2} \cdot \frac{\sinh^2(\alpha_1 l\,\omega_N)}{(\alpha_1 l)^2} e^{-2\alpha_0 l} \tag{28}$$

Since $\alpha_1\, l\, \omega_N$ is much smaller than 1 for DWGs in the mm-wave frequency range (see Section "Attenuation constant,") the small argument approximation of hyperbolic sine ($\sinh(x) \approx x$) can be applied. Thus, the SNR simplifies to

$$\text{SNR} \approx \frac{\sigma_D^2}{\sigma_N^2} \cdot e^{-2\alpha_0 l} \quad \text{for} \quad |\alpha_1 l\, \omega_N| \ll 1 \tag{29}$$

This clearly shows that the SNR at the receiver of a DWG-based transmission system is simply the SNR of a channel with purely additive white Gaussian-distributed noise (AWGN channel) reduced by the attenuation of the DWG. Thus, the effect of the frequency-dependent attenuation on the SNR is negligible.

In addition to the SNR, the ISI is of interest in order to determine the expected signal distortions along the transmission channel. Applying the definition of the ISI given by (5) leads to an analytical description of the ISI. The magnitude squared of the impulse response of the wanted signal $|h(0)|^2$ has already been given by (28). The sum of the magnitude squared of the impulse response of all signals that superimpose the wanted signal converges to

$$\sum_{\substack{k=-\infty \\ k\neq 0}}^{\infty} |h(kT)|^2 = \frac{1}{\omega_N^2} \cdot \sinh^2(\alpha_1 l \omega_N) e^{-2\alpha_0 l} \cdot \left[\frac{\omega_N}{\alpha_1 l}\coth(\alpha_1 l\,\omega_N) - \frac{1}{(\alpha_1 l)^2}\right] \tag{30}$$

(for derivation see Appendix A). Using (28) and (30) as well as the definition of the ISI given by (5) an analytical description of the ISI can be obtained:

$$\text{ISI} = \frac{1}{\alpha_1 l\, \omega_N \cdot \coth(\alpha_1 l\, \omega_N) - 1} \tag{31}$$

Figure 5(a) shows the ISI for the common range of Taylor coefficient α_1 in the mm-wave frequency range for different signal bandwidths $2f_N$ and a DWG length of $l = 1$ m. It can be seen that for typical values of the frequency-dependent attenuation in the mm-frequency range $\alpha_1 = 10^{-13}..10^{-11}$ s/m a tolerable ISI can be achieved for all bandwidths over a DWG length of $l = 1$ m. For example, the single-mode DWG made of PTFE given in Table I of 1 m length would still achieve a very good ISI of 33 dB even at a bandwidth of 20 GHz. Using a single-mode DWG made of PS reduces the ISI to 17 dB due to higher frequency dependency of the attenuation. With increasing length, the signal distortions further increase. For example, if the length is changed from 1 to 10 m, the ISI lowers by 20 dB. Therefore, for larger bandwidths and longer length l an optimization of the DWG toward low $\alpha_1 \leq 10^{-12}$ s/m is recommended. A detailed study is given in Section "DWG design for low signal distortions."

Distortions caused by dispersion

The frequency-dependent phase constant of DWGs is modeled by the Taylor coefficients β_0, β_1, and β_2, which includes the modeling of group delay and dispersion. This yields the baseband frequency transfer function given by (24). Applying the inverse Fourier transform according to (25) leads to the impulse response of the dispersive DWG channel

$$h(t) = \frac{T}{4\pi}\sqrt{\frac{\pi}{\gamma_2 l}} e^{\frac{(\gamma_1 l - jt)^2}{4\gamma_2 l} - \gamma_0 l} \cdot \left[\text{erf}\left(\frac{2\gamma_2 l\,\omega_N + \gamma_1 l - jt}{2\sqrt{\gamma_2 l}}\right) - \text{erf}\left(\frac{-2\gamma_2 l\,\omega_N + \gamma_1 l - jt}{2\sqrt{\gamma_2 l}}\right)\right] \tag{32}$$

where erf() represents the error function

$$\text{erf}(x) = \frac{2}{\sqrt{\pi}}\int_0^x e^{-\tau^2} d\tau. \tag{33}$$

Similar to Section "Distortions caused by attenuation," the Taylor coefficient β_1 is set to zero for further analysis, since it has no influence on the signal distortions. Accordingly, the magnitude squared of the wanted signal is

$$|h(0)|^2 = \frac{\pi}{16\omega_N^2}\frac{1}{|\beta_2| l} e^{-2\alpha_0 l} \cdot \left|\text{erf}\left(\frac{j2\beta_2 l\,\omega_N + \alpha_1 l}{2\sqrt{j\beta_2 l}}\right) - \text{erf}\left(\frac{-j2\beta_2 l\,\omega_N + \alpha_1 l}{2\sqrt{j\beta_2 l}}\right)\right|^2 \tag{34}$$

and the magnitude squared of the interfering signal is

$$\sum_{\substack{k=-\infty \\ k\neq 0}}^{\infty} |h(kT)|^2 = \frac{\pi}{16\omega_N^2}\frac{1}{|\beta_2| l} e^{-2\alpha_0 l} \cdot \sum_{k=-\infty k\neq 0}^{\infty} e^{-\frac{\alpha}{\beta_2}\frac{\pi}{\omega_N}k} \cdot \left|\text{erf}\left(\zeta_1(k)\right) - \text{erf}\left(\zeta_2(k)\right)\right|^2$$

https://doi.org/10.1017/S1759078721000209 Published online by Cambridge University Press

with

$$\zeta_1(k) = \frac{j2\beta_2 l\,\omega_N + \alpha_1 l - j\frac{\pi}{\omega_N}k}{2\sqrt{j\beta_2 l}}$$
$$\zeta_2(k) = \frac{-j2\beta_2 l\,\omega_N + \alpha_1 l - j\frac{\pi}{\omega_N}k}{2\sqrt{j\beta_2 l}} \quad (35)$$

The series (35) converges (for proof see Appendix B) and is therefore analyzed numerically to determine the ISI. First, the ISI is considered without the influence of frequency-dependent attenuation ($\alpha_1 = 0$). The results are shown in Fig. 5(b). A considerably greater effect on the ISI compared to the frequency-dependent attenuation can be observed in Fig. 5(a). Especially with increasing signal bandwidth the ISI increases significantly. For typical values of $|\beta_2| \leq 10^{-21}\,\mathrm{s^2/m^2}$, an acceptable ISI can only be achieved for smaller bandwidth and/or shorter length. If the single-mode DWG made of PTFE in Table I is considered, it can be seen that for a bandwidth of 20 GHz and a length of 1 m only an ISI in a range of $\approx 10..20$ dB is achieved. This is a significant reduction compared to the ISI caused by frequency-dependent attenuation. A transmission over $l \geq 10$ m seems only possible for smaller bandwidths (e.g. 5 GHz). However, as already shown in Section "Phase constant," the waveguide dispersion can be reduced to almost zero ($|\beta_2| \to 0$) for certain circular DWGs. In this case, the ISI and therefore the transmission length would be infinite. Since in practical application, the frequency-dependent attenuation is not negligible (see Section "Distortions caused by attenuation"), the question remains whether a minimized waveguide dispersion actually results in a low overall ISI.

DWG design for low signal distortions

As shown in Sections "Distortions caused by attenuation" and "Distortions caused by dispersion," frequency-dependent attenuation as well as waveguide dispersion have a significant effect on signals transmitted along a DWG. This is especially true for long distance communications ($l \geq 10$ m). However, it has also been shown that for certain circular DWGs, the waveguide dispersion vanishes completely ($\beta_2 = 0$). An interesting question at this point is whether this dispersion minimum really leads to minimal signal distortions despite frequency-dependent attenuation ($\alpha_1 \neq 0$). To answer this question, equation (35) is evaluated numerically for values of $\alpha_1 \neq 0$. In order to keep the variation of the results low, only a bandwidth of $2f_N = 5$ GHz is considered. The results for the ISI in dependency of α_1 and β_2 are shown in Fig. 5(c). It can be seen that for small values of α_1 ($\leq 10^{-15}$ s/m) the ISI as a function of α_1 and β_2 in Fig. 5(c) is almost congruent with the ISI in Fig. 5(b) ($B = 5$ GHz), where only dispersion caused by frequency-dependent group delay ($\alpha_1 = 0$) is considered. The influence of the frequency-dependent attenuation on the ISI can therefore be neglected for $\alpha_1 \leq 10^{-15}$ s/m. With increasing values of α_1, however, a limitation in the maximum achievable ISI appears despite negligible waveguide dispersion ($\beta_2 \leq 10^{-25}\,\mathrm{s^2/m^2}$). For example, a DWG with a Taylor coefficient of $\alpha_1 = 10^{-12}$ s/m and 1 m length leads to an ISI of ISI ≈ 41 dB even if the waveguide dispersion is zero. This limitation in the maximum achievable ISI despite negligible waveguide dispersion corresponds to the values determined for the attenuation-dependent ISI in Fig. 5(a) ($B = 5$ GHz). Whether the optimization

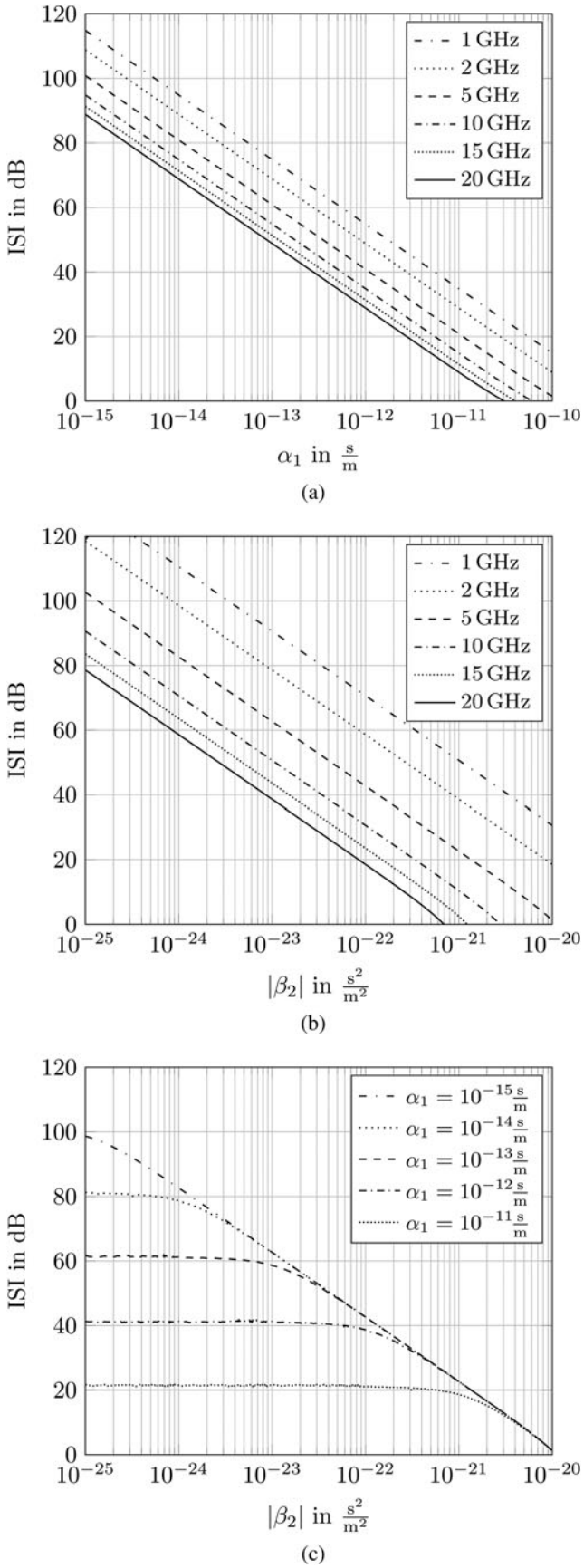

Fig. 5. ISI as a function of Taylor coefficient α_1 (a) and β_2 (b) for different signal bandwidths $2f_N$ as well as α_1 and β_2 (c) at a signal bandwidth of $2f_N = 5$ GHz.

https://doi.org/10.1017/S1759078721000209 Published online by Cambridge University Press

of a DWG to low waveguide dispersion also leads to a reduction of the expected ISI depends mainly on the frequency-dependent attenuation of the respective DWG. For example, for a DWG with a Taylor coefficient of $\alpha_1 = 10^{-12}$ s/m, reducing the waveguide dispersion below $|\beta_2| \leq 3 \times 10^{-23}$ s^2/m^2 would not further improve the ISI. This clearly shows that low signal distortions in DWGs can only be achieved if the frequency-dependent attenuation in addition to dispersion is reduced. This fact has not been considered in the majority of scientific studies so far. Furthermore, it is more challenging to reduce the frequency dependency of the attenuation than to reduce the waveguide dispersion of a DWG. Considering the mathematical description of the first-order frequency-dependent attenuation in (17), it is noticeable that the loss factors of core and cladding ($\tan\delta_1$, $\tan\delta_2$) occur with different prefactors. If both factors are considered separately, it can be seen that the prefactor of the cladding material's loss factor becomes negative for normalized frequencies of $V \geq 1.2$ (see Fig. 6). Thus, a minimization of the Taylor coefficient α_1 to zero is theoretically possible. However, a reduction of the frequency dependency of the attenuation is only possible if the cladding material has significantly higher losses than the core material ($\tan\delta_2 \approx 4 \,..\, 5 \times \tan\delta_1$). This would result in a significant increase of the total losses of the DWG and thus in a decrease of the SNR at the receiver.

It can generally be said that for low material ratios Δ the frequency dependency of attenuation and group delay is reduced and the signal distortions decrease. However, lower values of Δ also result in a lower field concentration in the core of the DWG (see Fig. 3(a)). This requires a larger size of the DWG package (core + cladding). In addition, the sensitivity to discontinuities will be increased. Therefore, a compromise on practical issues must be found when reducing Δ. In most of nowadays DWG applications, the relative permittivity of the used materials is in a range of $\varepsilon_r \approx 2{-}3$ and the loss factor in a range of $\tan\delta \approx 10^{-4}{-}10^{-3}$. Considering (17) and Fig. 6, the respective range of this Taylor coefficient is $\alpha_1 \approx 10^{-13}{-}10^{-11}$ s/m ($V \approx 2{-}3$). For such DWGs, a minimization of the waveguide dispersion is recommended, since it also reduces the frequency-dependent attenuation to an acceptable value. For the waveguide-dispersion-minimized DWG in Table I with a Taylor coefficient of $\alpha_1 = 6.0 \times 10^{-13}$ s/m, an ISI of ISI = 10 dB could still be achieved over lengths of 58 m (5 GHz bandwidth) or 14 m (20 GHz bandwidth). Reducing α_1 by a factor of 10 allows to increase the respective lengths by the same factor. For comparison, using the single-mode DWG made of PTFE in Table I with Taylor coefficients of $\alpha_1 = 6.4 \times 10^{-13}$ s/m and $\beta_2 = 2.0 \times 10^{-22}$ s/m would only achieve a transmission length of 19 m (5 GHz bandwidth) or 1.3 m (20 GHz bandwidth). This clearly shows the great potential of dispersion optimization of DWGs in the mm-wave frequency range.

Conclusion

In this paper, a detailed study of signal distortions due to frequency-dependent attenuation and group delay of DWGs in a low-complexity digital transmission system was presented. Based on a general description of this frequency dependency for circular DWGs, it was shown that both frequency-dependent attenuation as well as waveguide dispersion have a significant effect on the signal transmission. Although it is possible to reduce the waveguide dispersion to zero by proper waveguide design, the remaining frequency-dependent attenuation significantly limits the transmission capacity. It has also been shown that a complete compensation of this effect is only feasible if the cladding material of the DWG shows significantly higher losses than the core material. With the currently available materials, this would result in high transmission losses. However, reducing the frequency-dependent attenuation to an acceptable level can be achieved with the currently available materials, especially for dispersion-minimized DWGs. For this purpose, it is recommended to choose a core material with low permittivity and low losses (e.g. PTFE and PE) and at the same time a low material ratio Δ. Such improvements of the transmission channel allow to further reduce signal distortions and thus to further increase the maximum achievable data rates and transmission distances without the need of more complex transceivers.

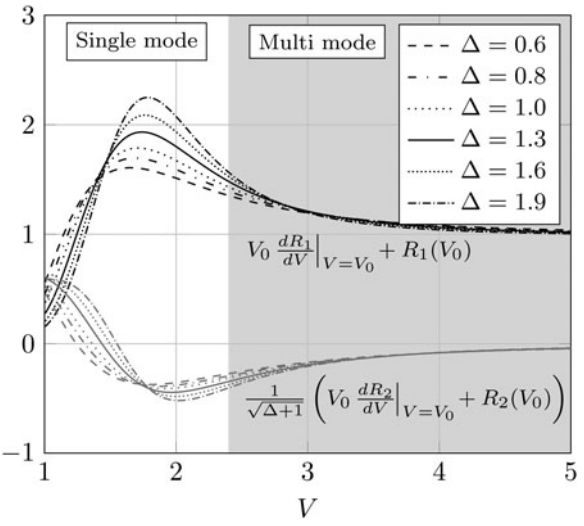

Fig. 6. Core and cladding material prefactor in (17) as a function of the normalized frequency V for different material ratios Δ.

References

1. **Fukuda S, Hino Y, Ohashi S, Takeda T, Yamagishi H, Shinke S, Komori K, Uno M, Akiyama Y, Kawasaki K and Hajimiri A** (2011) A 12.5+12.5 Gb/s full-duplex plastic waveguide interconnect. *IEEE Journal of Solid-State Circuits* **46**, 12, 3113–3125.
2. **De Wit M, Ooms S, Philippe B, Zhang Y and Reynaert P** (2020) Polymer microwave fibers: a new approach that blends wireline, optical, and wireless communication. *IEEE Microwave Magazine* **21**, 1, 51–66.
3. **Holloway JW, Dogiamis GC and Han R** (2020) Innovations in terahertz interconnects: high-speed data transport over fully electrical terahertz waveguide links. *IEEE Microwave Magazine* **21**, 1, 35–50.
4. **Sawaby M, Dolatsha N, Grave B, Chen C and Arbabian A** (2018) A fully packaged 130-GHz QPSK transmitter with an integrated PRBS generator. *IEEE Solid-State Circuits Letters* **1**, 7, 166–169.
5. **Van Thienen N, Zhang Y, De Wit M and Reynaert P** (2016) An 18Gbps polymer microwave fiber (PMF) communication link in 40 nm CMOS. *ESSCIRCConference 2016: 42nd European Solid-State Circuits Conference*, September, pp. 483–486.
6. **Thienen NV, Zhang Y and Reynaert P** (2018) Bidirectional communication circuits for a 120-GHz PMF data link in 40-nm CMOS. *IEEE Journal of Solid-State Circuits* **53**, 7, 2023–2031.
7. **Kim Y, Nan L, Cong J and Chang MF** (2013) High-speed mm-wave data-link based on hollow plastic cable and CMOS transceiver. *IEEE Microwave and Wireless Components Letters* **23**, 12, 674–676.
8. **Yu B, Liu Y, Ye Y, Liu X and Gu QJ** (2016) Low-loss and broadband G-band dielectric interconnect for chip-to-chip communication. *IEEE Microwave and Wireless Components Letters* **26**, 7, 478–480.

https://doi.org/10.1017/S1759078721000209 Published online by Cambridge University Press

9. **Van Thienen N, Volkaerts W and Reynaert P** (2016) A multi-gigabit CPFSK polymer microwave fiber communication link in 40 nm CMOS. *IEEE Journal of Solid-State Circuits* **51**, 8, 1952–1958.
10. **Yu B, Liu Y, Ye Y, Ren J, Liu X and Gu QJ** (2016) High-efficiency micromachined sub-THz channels for low-cost interconnect for planar integrated circuits. *IEEE Transactions on Microwave Theory and Techniques* **64**, 1, 96–105.
11. **Häseker JS and Schneider M** (2016) 90 degree microstrip to rectangular dielectric waveguide transition in the W-band. *IEEE Microwave and Wireless Components Letters* **26**, 6, 416–418.
12. **Yu B, Ye Y, Ding X, Liu Y, Xu Z, Liu X and Gu QJ** (2018) Ortho-mode sub-THz interconnect channel for planar chip-to-chip communications. *IEEE Transactions on Microwave Theory and Techniques* **66**, 4, 1864–1873.
13. **Dey U and Hesselbarth J** (2018) Building blocks for a millimeter-wave multiport multicast chip-to-chip interconnect based on dielectric waveguides. *IEEE Transactions on Microwave Theory and Techniques* **66**, 12, 5508–5520.
14. **Meyer A and Schneider M** (2020) Robust design of a broadband dual-polarized transition from PCB to circular dielectric waveguide for mm-wave applications. *International Journal of Microwave and Wireless Technologies* **12**, 7, 559–566.
15. **Dolatsha N, Chen C and Arbabian A** (2016) Loss and dispersion limitations in mm-wave dielectric waveguides for high-speed links. *IEEE Transactions on Terahertz Science and Technology* **6**, 4, 637–640.
16. **De Wit M, Zhang Y and Reynaert P** (2019) Analysis and design of a foam-cladded PMF link with phase tuning in 28-nm CMOS. *IEEE Journal of Solid-State Circuits* **54**, 7, 1960–1969.
17. **Meyer A, Krüger K and Schneider M** (2018) Dispersion-minimized rod and tube dielectric waveguides at W-band and D-band frequencies. *IEEE Microwave and Wireless Components Letters* **28**, 7, 555–557.
18. **Snitzer E** (1961) Cylindrical dielectric waveguide modes. *The Journal of the Optical Society of America* **51**, 5, 491–498.
19. **Yeh C and Shimabukuro FI** (2008) *The Essence of Dielectric Waveguides*. New York, USA: Springer.
20. **Meyer A, Turan B and Schneider M** (2018) Modal Dispersion Reduction in Multi-Mode Circular Dielectric Waveguides at W-band Frequencies. *2018 48th European Microwave Conference (EuMC)*, September, pp. 154–157.
21. **Heaviside O** (1925) *Electromagnetic Theory*. UK: Ernest Benn Ltd, p. 409.
22. **Zwillinger D, Moll V, Gradshteyn I and Ryzhik I** (eds) (2014) *Table of Integrals, Series, and Products*, 8th Edn. London, UK: Academic Press.

Appendix A. Derivation of ISI caused by frequency-dependent attenuation

The ISI caused by a frequency-dependent attenuation of a DWG is defined by (5) with (28) in the numerator and the infinite sum

$$\sum_{\substack{k=-\infty\\k\neq 0}}^{\infty}|h(kT)|^2=\sum_{k=-\infty k\neq 0}^{\infty}\frac{1}{\omega_N^2}\cdot\frac{\sinh^2(\alpha_1 l\,\omega_N)}{(\alpha_1 l)^2+(\frac{\pi}{\omega_N}k)^2}e^{-2\alpha_0 l} \tag{A.1}$$

in the denominator. This denominator can be rewritten as

$$\sum_{\substack{k=-\infty\\k\neq 0}}^{\infty}|h(kT)|^2=\sum_{k=-\infty}^{\infty}|h(kT)|^2-|h(0)|^2 \tag{A.2}$$

where $|h(0)|^2$ is given by (28) and

$$\begin{aligned}\sum_{k=-\infty}^{\infty}|h(kT)|^2&=\frac{1}{\omega_N^2}\cdot\sinh^2(\alpha_1 l\,\omega_N)e^{-2\alpha_0 l}\cdot\sum_{k=-\infty}^{\infty}\frac{1}{(\alpha_1 l)^2+\left(\frac{\pi}{\omega_N}k\right)^2}\\&=\frac{1}{\omega_N^2}\cdot\frac{\omega_N}{\alpha_1 l}\sinh^2(\alpha_1 l\,\omega_N)\coth(\alpha_1 l\,\omega_N)e^{-2\alpha_0 l}\end{aligned} \tag{A.3}$$

Thus

$$\sum_{\substack{k=-\infty\\k\neq 0}}^{\infty}|h(kT)|^2=\frac{1}{\omega_N^2}\cdot\sinh^2(\alpha_1 l\,\omega_N)e^{-2\alpha_0 l}\cdot\left[\frac{\omega_N}{\alpha_1 l}\coth(\alpha_1 l\,\omega_N)-\frac{1}{(\alpha_1 l)^2}\right] \tag{A.4}$$

Consequently, for the ISI follows

$$\mathrm{ISI}=\frac{|h(0)|^2}{\sum_{\substack{k=-\infty\\k\neq 0}}^{\infty}|h(kT)|^2}=\frac{1}{\alpha_1 l\,\omega_N\cdot\coth(\alpha_1 l\,\omega_N)-1} \tag{A.5}$$

Appendix B. Convergence of ISI caused by dispersion

To proof that the ISI caused by frequency-dependent attenuation and frequency-dependent group delay of a DWG can be calculated numerically, as it has been done in Section "Signal distortions," it is needed to proof its convergence. The ISI under influence of dispersion is defined by (5) with (34) in the numerator and (35) in the denominator. To verify that the infinite series in (35) converges, the series is first divided into two sums, each with a positive running index k. Afterward, the convergence of both sums is verified separately:

$$\begin{aligned}&\sum_{k=1}^{\infty}e^{-\frac{\alpha_1}{\beta_2}\frac{\pi}{\omega_N}k}\cdot\left|\mathrm{erf}\left(\zeta_1(k)\right)-\mathrm{erf}\left(\zeta_2(k)\right)\right|^2\\&\quad+\sum_{k=1}^{\infty}e^{\frac{\alpha_1}{\beta_2}\frac{\pi}{\omega_N}k}\cdot\left|\mathrm{erf}\left(\zeta_1(-k)\right)-\mathrm{erf}\left(\zeta_2(-k)\right)\right|^2\end{aligned} \tag{B.1}$$

The convergence of both sums in (B.1) can be verified by the comparison test which states that an infinite series $\sum_{n=0}^{\infty}a_n$ converges, if there is a convergent infinite series $\sum_{n=0}^{\infty}b_n$ for whose real summands holds: $|a_n|\leq|b_n|$ for all $n\geq n_0\in\mathbb{N}$, where n_0 can be any countable running index.

Using the triangle inequality

$$|z_1\pm z_2|\leq|z_1|+|z_2| \qquad \text{for} \qquad z_1,z_2\in\mathbb{C} \tag{B.2}$$

and the asymptotic expression of the error function [22]

$$\mathrm{erf}(z)\sim 1-\frac{e^{-z^2}}{\sqrt{\pi}z} \qquad \text{for} \qquad z\in\mathbb{C} \tag{B.3}$$

it can be stated for the summands of the first sum in (B.1) that

$$\begin{aligned}&\left|\mathrm{erf}\left(\zeta_1(k)\right)-\mathrm{erf}\left(\zeta_2(k)\right)\right|^2\cdot e^{-\frac{\alpha_1}{\beta_2}\frac{\pi}{\omega_N}k}\\&\leq\left[\left|\frac{e^{-\zeta_2(k)^2}}{\sqrt{\pi}\cdot\zeta_2(k)}\right|+\left|\frac{e^{-\zeta_1(k)^2}}{\sqrt{\pi}\cdot\zeta_1(k)}\right|\right]^2\cdot e^{-\frac{\alpha_1}{\beta_2}\frac{\pi}{\omega_N}k}\\&=\frac{1}{\pi}\left[\frac{e^{-\mathrm{Re}\{\zeta_2(k)^2\}-\frac{\alpha_1}{\beta_2}\frac{\pi}{2\omega_N}k}}{|\zeta_2(k)|}+\frac{e^{-\mathrm{Re}\{\zeta_1(k)^2\}-\frac{\alpha_1}{\beta_2}\frac{\pi}{2\omega_N}k}}{|\zeta_1(k)|}\right]^2\end{aligned} \tag{B.4}$$

In order to fulfill the comparison test, it is necessary to verify whether the sum

$$\sum_{k=1}^{\infty}\left[\frac{e^{-\mathrm{Re}\{\zeta_2(k)^2\}-\frac{\alpha_1}{\beta_2}\frac{\pi}{2\omega_N}k}}{|\zeta_2(k)|}+\frac{e^{-\mathrm{Re}\{\zeta_1(k)^2\}-\frac{\alpha_1}{\beta_2}\frac{\pi}{2\omega_N}k}}{|\zeta_1(k)|}\right]^2 \tag{B.5}$$

actually converges. This can be verified by the ratio test which states that an infinite series $\sum_{n=0}^{\infty}b_n$ converges if its summands satisfy: $|(b_{n+1})/(b_n)|<1$

https://doi.org/10.1017/S1759078721000209 Published online by Cambridge University Press

for $n \geq n_0 \in \mathbb{N}$. Thus,

$$\frac{\frac{e^{-\mathrm{Re}\{\zeta_2(k+1)^2\}-\frac{\alpha_1}{\beta_2}\frac{\pi}{2\omega_N}(k+1)}}{|\zeta_2(k+1)|}+\frac{e^{-\mathrm{Re}\{\zeta_1(k+1)^2\}-\frac{\alpha_1}{\beta_2}\frac{\pi}{2\omega_N}(k+1)}}{|\zeta_1(k+1)|}}{\frac{e^{-\mathrm{Re}\{\zeta_2(k)^2\}-\frac{\alpha_1}{\beta_2}\frac{\pi}{2\omega_N}k}}{|\zeta_2(k)|}+\frac{e^{-\mathrm{Re}\{\zeta_1(k)^2\}-\frac{\alpha_1}{\beta_2}\frac{\pi}{2\omega_N}k}}{|\zeta_1(k)|}}<1 \tag{B.6}$$

with

$$\mathrm{Re}\{\zeta_1(k)^2\}=\alpha_1\omega_N-\frac{\alpha_1}{\beta_2}\frac{\pi}{2\omega_N}k, \tag{B.7}$$

$$\mathrm{Re}\{\zeta_2(k)^2\}=-\alpha_1\omega_N-\frac{\alpha_1}{\beta_2}\frac{\pi}{2\omega_N}k, \tag{B.8}$$

$$|\zeta_1(k)|=\sqrt{\frac{\alpha_1^2}{4|\beta_2|}+\frac{\pi^2k^2}{4|\beta_2|\omega_N^2}-\frac{\pi|\beta_2|k}{\beta_2}+|\beta_2|\omega_N^2}, \tag{B.9}$$

$$|\zeta_2(k)|=\sqrt{\frac{\alpha_1^2}{4|\beta_2|}+\frac{\pi^2k^2}{4|\beta_2|\omega_N^2}+\frac{\pi|\beta_2|k}{\beta_2}+|\beta_2|\omega_N^2}. \tag{B.10}$$

Equation (B.6) simplifies to

$$\frac{\frac{e^{\alpha_1\omega_N}}{|\zeta_2(k+1)|}+\frac{e^{-\alpha_1\omega_N}}{|\zeta_1(k+1)|}}{\frac{e^{\alpha_1\omega_N}}{|\zeta_2(k)|}+\frac{e^{-\alpha_1\omega_N}}{|\zeta_1(k)|}}<1. \tag{B.11}$$

It can be directly seen that with increasing running index k the numerator in (B.11) decreases faster than the denominator. Thus, the series (B.5) must have a non-countable set of summands with the running index $k > k_0$ that fulfill condition (B.11). As a result, the series (B.5) and therefore the first sum in (B.1) converges. Since the proof given for the first sum in (B.1) also holds for the second sum, equation (B.1) converges. Obviously, the convergence of series (B.1) is also valid for the case $\alpha_1 = 0$, as used in Section "Distortions caused by dispersion."

Andre Meyer received his Diploma degree in Communication and Information Technology from the University of Bremen, Germany in 2015. He is currently a research engineer at the RF & Microwave Engineering Laboratory of the University of Bremen, working toward his Ph.D. degree in high data-rate transmission systems using dielectric waveguides.

Martin Schneider received his Diploma and Doctorate degree in Electrical Engineering from the University Hanover, Germany, in 1992 and 1997, respectively. From 1997 to 1999, he was with Bosch Telecom GmbH, where he developed microwave components for point-to-point and point-to-multipoint radio link systems. In November 1999, he joined the Corporate Research division of Robert Bosch GmbH. As a project and section manager of the "Wireless Systems" group he focused on research and development of smart antenna concepts for automotive radar sensors at 24 and 77 GHz. From 2005 to 2006, he was with the business unit "Automotive Electronics" of Robert Bosch GmbH where he was responsible for the "RF electronics" of automotive radar sensors. Since March 2006, he has been a full professor and head of the RF & Microwave Engineering Laboratory at the University of Bremen (Germany).

https://doi.org/10.1017/S1759078721000209 Published online by Cambridge University Press